JOURNAL OF GUIDANCE, CONTROL, AND DYNAMICS
Vol. 19, No. 1, January–February 1996

Linear Quadratic Flight Control for Ejection Seats

Kevin A. Wise and Joseph S. Brinker
McDonnell Douglas Aerospace, St. Louis, Missouri 63166

A linear quadratic based flight control design for a next generation ejection seat design is presented. The flight control design process, dynamic models, control algorithm design, and nonlinear simulation results are presented. The study results are for a solid fuel pintle-based propulsion actuation system. The controller design was verified through linear analysis and nonlinear six-degree-of-freedom simulation.

Introduction

THE results presented in this paper support flight control system trade studies for the fourth generation escape system technology demonstration program.[1] The objective of this program is to demonstrate technologies that will enable safe escape from high-performance aircraft at high speeds,[1–4] with a focus on a controllable propulsion system and life support devices.

The ejection seat escape system requires a flight control design that satisfies high-performance specifications and guarantees stability at all times.[4] Although these requirements sound typical of most flight control systems, the escape system flight control requirements are very different from those of missiles and piloted aircraft. High maneuver rates are needed to ensure a safe separation. This requires a high bandwidth control design. The large flight envelope and aerodynamic[5,6] and mass property uncertainties require the flight control system to be very robust. In general, performance is usually sacrificed for robustness. For this reason a thorough trade study to evaluate the impact of the control algorithms on performance and robustness is needed.

Modern control techniques have successfully been applied to numerous missile and aircraft flight control designs[7–10]; however, less experience exists in applying these techniques to ejection seats. These problems have historically been approached using classical control design techniques and nonlinear simulation analysis.[11,12] Advanced sensors, such as ground proximity guidance systems,[13] facilitate the design of guidance systems to accommodate highly dynamic ejection scenarios. The high bandwidth flight control system required by these guidance strategies presents a significant design challenge using classical techniques. A linear quadratic approach to this design problem will be presented in this paper.

Guidance

The goal of the guidance and control algorithms is to maximize chute deployment altitude, maintain a low-risk multiaxial dynamic response criteria (MDRC), and minimize wind blast effects at high speeds. Figure 1 illustrates the MDRC acceleration limits for high, medium, and low risks of injury. The guidance strategy employed controls MDRC by scheduling angle of attack (AOA) and regulating sideslip. Sideslip regulation minimizes lateral accelerations, to which MDRC is most sensitive. AOA schedules were optimized through nonlinear 6-degree-of-freedom (DOF) simulation to balance the axial and normal acceleration contributions to MDRC, the minimization of wind blast effects, and the maximization of chute deployment altitude.

The guidance commands are separated into pitch-plane commands and lateral-directional commands. The pitch-plane command is scheduled with speed, transitioning from attitude control at low speeds to AOA control at high speeds. In the lateral directional axes, body roll attitude is regulated to zero to orient the seat with the vertical, and sideslip is regulated to minimize lateral accelerations.

At ejection speeds below 400-knots equivalent air speed (KEAS), attitude control is employed to align the thrust vector in a vertical direction to maximize altitude. At higher speeds, AOA control is employed to align the wind flow vector to minimize MDRC and wind

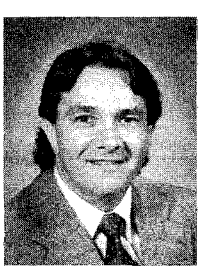

Kevin A. Wise is a Senior Principal Technical Specialist in the New Aircraft and Missile Products division of McDonnell Douglas Aerospace (MDAE) and Adjunct Assistant Professor in Electrical Engineering at the University of Missouri–Rolla and Southern Illinois University Edwardsville. He received his B.S.M.E. (1980), M.S. (1982), and Ph.D. (1987) from the University of Illinois. Since joining MDAE in 1982, Dr. Wise has been actively involved in the application of modern estimation and control theory in navigation and flight control problems. He has supported programs analyzing optimal guidance laws for terminal homing missiles, digital processing requirements for factorized Kalman filter algorithms, GPS aided inertial navigation systems, and flight control design for aircraft, missiles, unmanned air vehicles, and ejection seats.

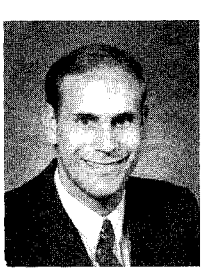

Joseph S. Brinker is a Senior Project Engineer in the New Aircraft and Missile Products division of McDonnell Douglas Aerospace (MDAE) and Adjunct Lecturer in Electrical Engineering at Southern Illinois University at Edwardsville. He received his B.S.E.E. (1988), B.S. Mathematics (1988), and M.S.E.E. (1990) from Southern Illinois University at Edwardsville. Since joining MDAE in 1988, Mr. Brinker has been actively involved in the application of modern estimation and control theory in guidance and flight control problems. His current efforts are focused on the design and analysis of flight control systems for aircraft, missiles, and ejection seats.

Received Feb. 8, 1995; revision received Aug. 5, 1995; presented as Paper 95-3320 at the AIAA Guidance, Navigation, and Control Conference, Baltimore, MD, Aug. 7–10, 1995; accepted for publication Aug. 10, 1995.

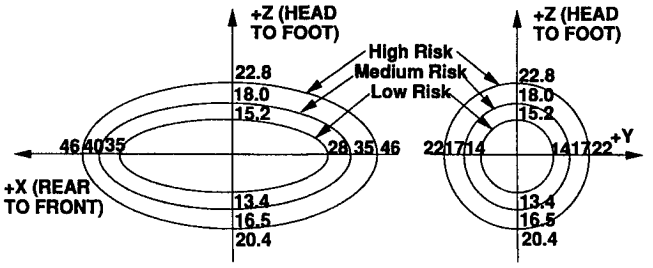

Fig. 1 Acceleration limits for pilot safety. Multiaxial dynamic response criteria (MDRC) $\sim g$.

blast effects while still providing a vertical component of thrust. The AOA command is scheduled with air speed to satisfy MDRC constraints. As air speed increases, it is desirable for the pilot to be in a more upright position for both MDRC and wind blast considerations.

Ejection Seat Dynamics

The body axis equations of motion (EOM) are used to model the escape system dynamics. A rigid body with constant mass and inertia is assumed. The standard 6-DOF body EOM are written as

$$\begin{aligned}
\dot{u} &= rv - qw + G_x + X_A + X_T \\
\dot{v} &= pw - ru + G_y + Y_A + Y_T \\
\dot{w} &= qu - pv + G_z + Z_A + Z_T \\
\dot{p} &= -L_{pq}pq - L_{qr}qr + L + L_T \\
\dot{q} &= -M_{pr}pr - M_{p^2r^2}(r^2 - p^2) + M + M_T \\
\dot{r} &= -N_{pq}pq - N_{qr}qr + N + N_T
\end{aligned} \tag{1}$$

where (G_x, G_y, G_z) (feet per second squared) models gravity, (X_A, Y_A, Z_A) (feet per second squared) models aerodynamic accelerations, (L, M, N) (radian per second squared) models aerodynamic moments along the appropriate axis, respectively, (X_T, Y_T, Z_T) (feet per second squared) models thrust forces (T_x, T_y, T_z) (pound) normalized with respect to the mass, and (L_T, M_T, N_T) (radian per second squared) models the moments produced by the thrust (M_x, M_y, M_z) (foot-pound) normalized by the inertia matrix. The aerodynamic forces are modeled as nondimensional forces and are scaled to units of force. These forces and moments are modeled as functions of AOA, β, Mach, and whether the propulsion system is on or off. The pitch-plane AOA α and yaw-plane sideslip angle β are defined following standard definitions that can be found in McRuer et al.[14]

In the design of the flight control laws, differential equations for α and β are used rather than the translation velocities expressed in Eq. (1). The body velocities u, v, and w are $u = V\cos(\alpha)\cos(\beta)$, $v = V\sin(\beta)$, and $w = V\sin(\alpha)\cos(\beta)$. Differentiating and equating to Eq. (1) results in

$$\begin{aligned}
\dot{\alpha} &= \frac{1}{V\cos(\beta)}\{\cos(\alpha)[G_z + Z_A + Z_T] \\
&\quad - \sin(\alpha)[G_x + X_A + X_T]\} + q \\
&\quad - \{p\cos(\alpha) + r\sin(\alpha)\}\tan(\beta) \\
\dot{\beta} &= (1/V)\{-\cos(\alpha)\sin(\beta)[G_x + X_A + X_T] \\
&\quad + \cos(\beta)[G_y + Y_A + Y_T] - \sin(\alpha)\sin(\beta)[G_z + Z_A + Z_T]\} \\
&\quad + p\sin(\alpha) - r\cos(\alpha)
\end{aligned} \tag{2}$$

Aerodynamic models of the ejection seat indicate that as long as the sideslip angle remains small the pitch aerodynamics can be decoupled from the lateral-directional aerodynamics. This results in the following pitch and roll-yaw linear control law design models.

Pitch:

$$\begin{bmatrix} \dot{\theta} \\ \dot{q} \\ \dot{\alpha} \end{bmatrix} = \begin{bmatrix} 0 & 1 & 0 \\ 0 & 0 & \left.\frac{\partial M}{\partial \alpha}\right|_{\alpha_0} \\ \frac{g\sin(\alpha_0)}{V} & 1 & \frac{Z_\alpha}{V} \end{bmatrix} \begin{bmatrix} \theta \\ q \\ \alpha \end{bmatrix} + \begin{bmatrix} 0 & 0 & 0 \\ 0 & 0 & \frac{1}{I_{yy}} \\ \frac{-\sin(\alpha_0)}{mV} & \frac{\cos(\alpha_0)}{mV} & 0 \end{bmatrix} \begin{bmatrix} T_x \\ T_z \\ M_y \end{bmatrix} \tag{3}$$

Roll-yaw:

$$\begin{bmatrix} \dot{\phi} \\ \dot{\psi} \\ \dot{p} \\ \dot{r} \\ \dot{\beta} \end{bmatrix} = \begin{bmatrix} 0 & 0 & 1 & 0 & 0 \\ 0 & 0 & 0 & 1 & 0 \\ 0 & 0 & 0 & 0 & \left.\frac{\partial L}{\partial \beta}\right|_{\alpha_0} \\ 0 & 0 & 0 & 0 & \left.\frac{\partial N}{\partial \beta}\right|_{\alpha_0} \\ \frac{g}{V} & 0 & \sin(\alpha_0) & -\cos(\alpha_0) & \frac{Y_\beta}{V} \end{bmatrix} \begin{bmatrix} \phi \\ \psi \\ p \\ r \\ \beta \end{bmatrix} + \begin{bmatrix} 0 & 0 & 0 \\ 0 & 0 & 0 \\ 0 & \frac{I_{zz}}{I_{xx}I_{zz} - I_{xz}^2} & \frac{I_{xz}}{I_{xx}I_{zz} - I_{xz}^2} \\ 0 & \frac{I_{xz}}{I_{xx}I_{zz} - I_{xz}^2} & \frac{I_{xx}}{I_{xx}I_{zz} - I_{xz}^2} \\ \frac{1}{mV} & 0 & 0 \end{bmatrix} \begin{bmatrix} T_y \\ M_x \\ M_z \end{bmatrix} \tag{4}$$

where

$$Z_\alpha = \cos(\alpha_0)\left[\left\{\left(\frac{\partial Z_A}{\partial \alpha}\right) - X_A\right\}\Big|_{\alpha_0} - X_{T_0}\right] - \sin(\alpha_0)\left[\left\{\left(\frac{\partial X_A}{\partial \alpha}\right) + g + Z_A\right\}\Big|_{\alpha_0} + Z_{T_0}\right]$$

$$Y_\beta = \left.\frac{\partial Y_A}{\partial \beta}\right|_{\alpha_0} - \cos(\alpha_0)\left[\{X_A\}|_{\alpha_0} + X_{T_0}\right] - \sin(\alpha_0)\left[\{g + Z_A\}|_{\alpha_0} + Z_{T_0}\right]$$

Imbedded in these design models are mass properties for the pilot that depend on the size of the pilot. Table 1 lists the mass properties for both a 5 and 95% male crew member. A 50% male crew member mass properties were used for control law design.

Figure 2 illustrates the escape system with pintle ejection propulsion system[15] (PEPS) with the ejection seat performing a pitch up

Table 1 Escape system (seat and pilot) mass properties

Crew member percentile, %	5	95
Weight, lb	379.67	456.47
X c.g., ft	0.800	0.912
Y c.g., ft	−0.002	−0.002
Z c.g., ft	−1.316	−1.321
I_{xx}, slug-ft^2	19.63	23.62
I_{yy}, slug-ft^2	19.01	23.52
I_{zz}, slug-ft^2	6.80	9.11
I_{xy}, slug-ft^2	−0.024	−0.019
I_{xz}, slug-ft^2	2.52	2.89
I_{yz}, slug-ft^2	0.004	0.006

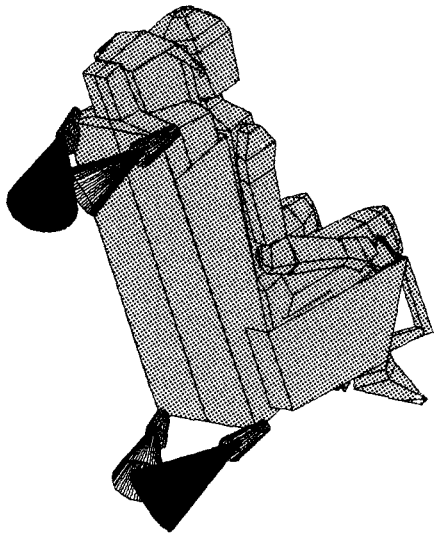

Fig. 2 Ejection seat with PEPS.

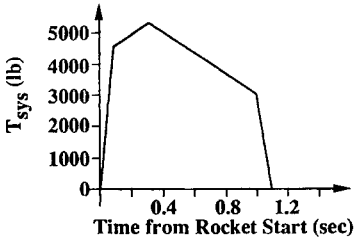

Fig. 3 PEPS system thrust duty cycle.

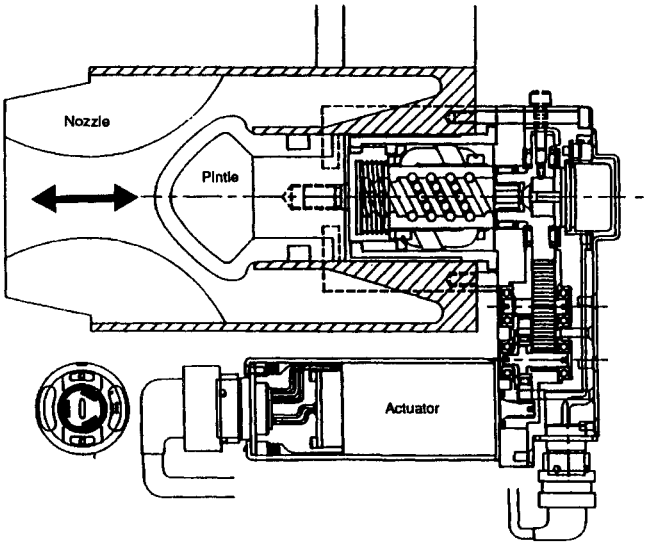

Fig. 4 PEPS actuator and pintle subsystem.

maneuver. The figure illustrates the location and geometry of the thrusters used to control the seat dynamics. The four thrusters (thrust levels) can be controlled independently, subject to the sum of all four thrust levels equaling the total system thrust $T_{sys}(t)$ shown in Fig. 3. Each thruster is controlled by moving a pintle into the throat of the nozzle using an electromechanical (EM) actuator. Figure 4 shows the EM actuator and pintle in greater detail. The thrust profile for the PEPS is shaped by the solid fuel grain design, and lasts approximately 1.1 s in duration.

Control Law Design

Two linear quadratic regulator (LQR) control laws were examined as part of the trade studies. The design approach is called the robust servomechanism LQR.[16] Both LQR designs (Fig. 5) used integral (I) control acting on the command error with proportional state feedback for stabilization. Integral control adds 90 deg of phase lag across all frequencies, which has a tendency to slow down the response and reduce command overshoot. The first LQ design examined used only integral control on the command error. The second design used both proportional and integral (PI) control on the command error. The added proportional control provides a quick response, whereas the integral control eliminates command errors.

Table 2 Flight control design guidelines

Stability margins, dB	>6 gain
deg	>30 phase
AOA limits, deg	±90
Rate limits, deg/s	±1000 (gyro limit)
G limits, g	±13 (lateral/normal)
	±28 (longitudinal)
Sample rate, H_2	600
Gain scheduling rate, H_2	600
Rise time, s	0.1
Settling time, s	0.2–0.3
Side slip regulation, s	0.1
Velocity range	$<M2.0$
Altitude range, Kft	< 20
Dynamic pressure range, psf	<3000
Mass parameters	50% crew member

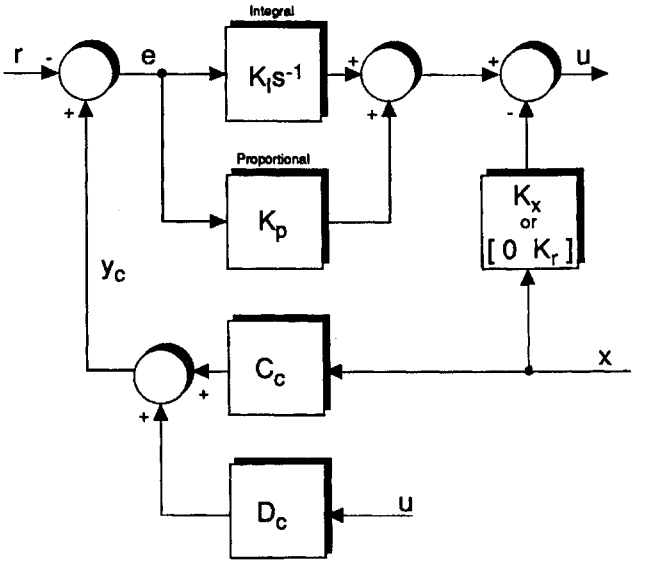

Fig. 5 LQR with proportional and integral error control.

The guidelines listed in Table 2 were used in the control law design.

Robust Servomechanism LQR Design

The robust servo LQR design uses integral control to track commands with zero steady-state error. The name robust comes from its ability to track any magnitude command, without altering the structure or feedback gains. The mechanization of the robust servo LQR algorithms allows for easy change of the commanded variable (i.e., attitude, rate, AOA, or acceleration) with no change in structure. This greatly simplifies the transition between different flight regimes where the commanded variable is changed, and allows for automation of the control law design.

Consider the following state-space model of the ejection seat dynamics:

$$\dot{x} = Ax + Bu$$
$$y_c = C_c x + D_c u \tag{5}$$

The command input vector $r(t)$ has the same dimension as y_c. Define the error signal as $e = y_c - r$. Tracking in y_c is regulation in e; therefore, the objective is to make the error approach zero $e \rightarrow 0 (y_c \rightarrow r)$ as $t \rightarrow \infty$, in a robust manner with respect to the plant

description. Incorporating integral error control, a new state-space system is defined as

$$\dot{z} = \tilde{A}z + \tilde{B}\mu \tag{6}$$

where

$$z = \begin{bmatrix} e \\ x \end{bmatrix}, \quad \mu = \dot{u}, \quad \tilde{A} = \begin{bmatrix} 0 & C_c \\ 0 & A \end{bmatrix}, \quad \tilde{B} = \begin{bmatrix} D_c \\ B \end{bmatrix} \tag{7}$$

LQR control theory is applied to Eq. (6) using the performance index (PI)

$$J = \int_0^\infty (z^T Q z + \mu^T R \mu)\, d\tau \tag{8}$$

The optimal state feedback control law for μ is formed by solving the algebraic Riccati equation[9,10] (ARE) using Q and R from Eq. (8). The resulting steady-state feedback controller gain matrix K is partitioned as $K = [K_I \;\; K_x]$, where K_I multiplies the integral of the command error vector and K_x multiplies the feedback of the states. The optimal control $u(t)$ is obtained by integrating $\mu(t)$, that is,

$$u = \int \mu d\tau = -K \int z d\tau = -K_I \int e d\tau - K_x x$$

This controller mechanization yields integral control action on the command error to provide zero steady-state error command following. The state vector x must be available for feedback. The implementation of this state feedback design is shown in Fig. 5.

This approach can be modified to provide both proportional and integral control on the command error by applying robust servo LQR theory to a modified plant model.[17] This approach models the plant using command errors as states. The performance index structure of Eq. (8) remains unchanged. Solution of the ARE yields a feedback gain matrix that can be partitioned as $K = [K_I \;\; K_p \;\; K_r]$, where K_I multiplies the integral of the command error, K_p multiplies the command error, and K_r multiplies the remaining feedback states. The optimal control $u(t)$ is obtained by integrating $\mu(t)$, that is,

$$u = \int \mu\, d\tau = -K \int z\, d\tau = -K_I \int e\, d\tau - K_p e - K_r x_r$$

This controller mechanization yields proportional and integral control action on the command error to provide zero steady-state error command following and a high bandwidth response. The implementation of this state feedback design is also shown in Fig. 5.

The control law gains are scheduled with Mach, AOA, and dynamic pressure. Root locus analyses of the open-loop dynamics were used to assess the sensitivity to these scheduling parameters over a flight envelope defined by the sled test launch conditions ($0 \le M \le 2.0$, $0 \le \bar{q} \le 3000$ psf, $|\alpha| < 90$ deg). These sensitivities were used to define the gain table break points.

The flight control laws utilize inertial measurement unit (IMU) measured body accelerations and angular rates as feedbacks. These measurements are filtered to reduce noise and to remove any flexible body dynamics. The IMU provides measured acceleration and rate data at 600 Hz.

To evaluate seat controllability and maneuverability, the maximum α and β that can be achieved with limited thrust levels are computed. These α, β maps represent a trimmed (zero moment) condition where at least one of the thrusters is saturated at its maximum thrust level. This contour shows the maximum α and β that can be commanded and is used to define command limits for the controller. Outside of these contours the seat is not controllable (the aerodynamic moments exceed the moments produced by the thrusters). Also computed are the aerodynamic loads that indicate the acceleration levels that can be achieved.

Figure 6 shows example trim α, β maps at a high-velocity flight condition for the PEPS system. These results were used in the early stages of this program to aid in sizing the propulsion system.

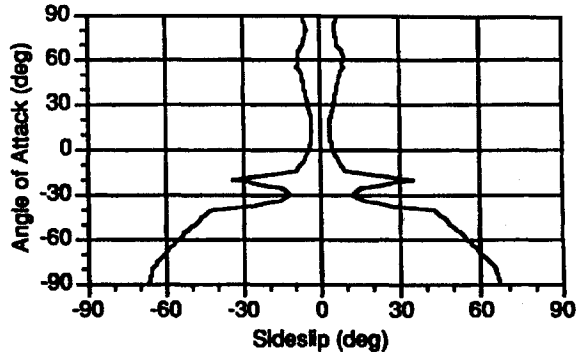

Fig. 6 AOA and sideslip limits for trimmed moments. Total thrust = 5000 lb, max thrust/nozzle = 2500 lb.

Robust Servo LQR Controller Design

The escape system flight control design was accomplished by applying robust servo LQR theory to the linearized plant models of Eqs. (3) and (4). Several LQR formulations were considered with the selected approach being a PI controller architecture designed by treating the thrust forces as disturbances in the AOA and sideslip dynamics. Considerations for selecting this approach are discussed in this section. Robust servo LQR formulations for the design of pitch attitude, AOA, and roll-yaw controllers are also provided.

The linearized plant models of Eqs. (3) and (4) have control inputs consisting of thrust forces and moments generated by the propulsion system. Application of robust servo LQR theory to these plant models yields a controller that commands both thrust forces and moments; however, this formulation is undesirable for several reasons. First, this approach treats the thrust forces and moments as independent controls, whereas in reality they are highly coupled since the thrust moments are generated by the thrust forces acting through appropriate moment arms (distance between the thruster location and the vehicle c.g.). Second, the nonlinear propulsion system thrust constraints can not be imbedded in this design model. The LQR controller will employ body axis thrust force commands, which may be positive or negative, to minimize the performance index of Eq. (8). These commands are inconsistent with the solid fuel propulsion system design and fixed thruster orientation that result in a predetermined thrust force profile along the x and z body axes.

These difficulties are overcome by designing a controller that commands only thrust moments and employing a thrust distribution function to select individual thruster commands that best satisfy the moment commands while obeying the propulsion system constraints. To design a moment command controller using robust servo LQR theory, the linearized plant dynamics of Eqs. (3) and (4) must be modified to have only thrust moment inputs.

One approach for accomplishing this is to use a matrix pseudoinverse based on the thrust force-moment relationships to create a plant model whose inputs are effective thrust moments. That is, thrust moments that capture the thrust force effects on the dynamics. The thrust forces along the body axes are related to the individual thruster forces as

$$\begin{bmatrix} T_x \\ T_y \\ T_z \end{bmatrix} = [u_1 \;\; u_2 \;\; u_3 \;\; u_4] \begin{bmatrix} T_1 \\ T_2 \\ T_3 \\ T_4 \end{bmatrix} = M_1 \begin{bmatrix} T_1 \\ T_2 \\ T_3 \\ T_4 \end{bmatrix} \tag{9}$$

where each u_i is a three-element (column) unit vector based on the angular orientation of thruster T_i with respect to the body axes. Similarly, the body axis thrust moments generated by the propulsion system are given by

$$\begin{bmatrix} M_x \\ M_y \\ M_z \end{bmatrix} = [\ell_1 \times u_1 \;\; \ell_2 \times u_2 \;\; \ell_3 \times u_3 \;\; \ell_4 \times u_4] \begin{bmatrix} T_1 \\ T_2 \\ T_3 \\ T_4 \end{bmatrix}$$

$$= M_2 \begin{bmatrix} T_1 \\ T_2 \\ T_3 \\ T_4 \end{bmatrix} \tag{10}$$

where ℓ_i represents the vector distance from the force application point of thruster T_i to the vehicle center of gravity.

Equations (9) and (10) allow the linearized dynamics of Eqs. (3) and (4) to be expressed in terms of the individual thruster commands. Equation (10) can also be used to compute a set of effective moment commands ($\bar{M}$) that best capture the dynamic effects of the individual thruster commands. A least squares solution of Eq. (10), for the underdetermined case, yields

$$\begin{bmatrix} T_1 \\ T_2 \\ T_3 \\ T_4 \end{bmatrix} = M_2^T \left(M_2 M_2^T\right)^{-1} \begin{bmatrix} \bar{M}_x \\ \bar{M}_y \\ \bar{M}_z \end{bmatrix} \tag{11}$$

Combining Eq. (11) with Eqs. (9) and (10) produces

$$\begin{bmatrix} T_x \\ T_y \\ T_z \\ M_x \\ M_y \\ M_z \end{bmatrix} = \begin{bmatrix} M_1 M_2^T \left(M_2 M_2^T\right)^{-1} \\ I \end{bmatrix} \begin{bmatrix} \bar{M}_x \\ \bar{M}_y \\ \bar{M}_z \end{bmatrix} \tag{12}$$

and allows the linearized dynamics models of Eqs. (3) and (4) to be expressed in terms of effective thrust moment inputs.

Application of robust servo LQR theory to these modified plant models produces the desired moment command controller; however, the matrix pseudoinverse approach suffers from similar downfalls as the formulation that commanded thrust forces and moments as independent controls. The effective moment commands implicitly model the thrust force commands, but can not impose the nonlinear propulsion system constraints on the individual thruster force levels. In addition, this approach was found to ill condition the LQR problem formulation and cause numerical difficulties in the solution of the ARE.

Another approach for designing a moment command controller is to use dynamic inversion[8] to cancel the thrust force dynamics of Eqs. (3) and (4). This formulation was not pursued due to large uncertainties in the ejection seat mass properties with crew member percentile. Dynamic inversion was employed to cancel the gyroscopic nonlinearities in the EOM, but was found to have negligible influence on the nonlinear escape sequence trajectories analyzed.

The selected design approach was to treat the thrust forces of Eqs. (3) and (4) as disturbances, and design a moment command controller that is robust to these disturbances. The linearized plant model used for this design approach is obtained by simply ignoring the columns of the B matrices of Eqs. (3) and (4) that correspond to the thrust forces. This formulation leads to indirect control of AOA and sideslip through the vehicle attitude and rotational rates, while providing a feasible approach for designing a controller that satisfies the propulsion system constraints. These constraints are eliminated from the LQR controller design and handled by the thrust distribution function. The application of robust servo LQR theory to these plant models leads to the desired controller architecture.

Our initial approach was to use robust servo LQR theory to design integral control topologies for pitch attitude, AOA, and roll-yaw control. Nonlinear simulation with this controller design revealed difficulty in initializing the integrators to prevent adverse transients in highly dynamic ejection scenarios. The PI controller formulation alleviated these concerns by allowing the integrator to be initialized to zero and by having the initial moment commands generated based on the command error and state feedbacks. This topology was used to generate the data presented in this paper.

Robust Servo LQR Pitch Attitude Controller Design

The ejection seat flight control system employs pitch attitude control at low speeds to orient the thrust vector to maximize chute deployment altitude. For pitch attitude control, the controlled output $\boldsymbol{y}_c$ is the body pitch attitude whereas the reference input $\boldsymbol{r}$ is the pitch attitude command. The command error becomes $\boldsymbol{e} = \theta - \theta_c$. The LQR design problem centers around the selection of the weighting matrices Q and R to yield the desired stability and performance characteristics across the flight envelope. The LQR performance index employed for this design is given by

$$J = \int_0^\infty q_1[(\varepsilon\theta)^2 + K(\varepsilon\dot{\theta})^2] + \dot{M}_y^2 \mathrm{d}t \tag{13}$$

The $\varepsilon\theta$ term of Eq. (13) penalizes the command error to provide command following, the $\varepsilon\dot{\theta}$ term drives the rate of change of the command error to zero to regulate command overshoot, and the $\dot{M}_y$ term penalizes the control effort employed. LQR design charts[18] were used at the corners of the flight envelope to select a value of K in Eq. (13) that allowed the desired stability and transient response characteristics to be achieved with some q_1. This value of K was then held fixed, and q_1 was varied at each design point to select controller gains that satisfied the flight control design goals.

Robust Servo LQR AOA Controller Design

The ejection seat flight control system employs AOA control at high speeds to control MDRC and minimize wind blast effects. For AOA control, the controlled output $\boldsymbol{y}_c$ is the body AOA, whereas the reference input $\boldsymbol{r}$ is the AOA command. The command error becomes $\boldsymbol{e} = \alpha - \alpha_c$. The LQR performance index was selected to be

$$J = \int_0^\infty q_1[(\varepsilon\alpha)^2 + K(\varepsilon\dot{\alpha})^2] + \dot{M}_y^2 \mathrm{d}t \tag{14}$$

This performance index is comparable to that of Eq. (13) and was used to design the controller gains in a manner analogous to that used for the pitch attitude controller.

Robust Servo LQR Roll-Yaw Controller Design

The ejection seat flight control system employs a roll-yaw controller that controls roll attitude for thrust vector orientation while regulating sideslip to minimize MDRC. The roll attitude control transitions from a body roll attitude at low speeds to a stability axis roll attitude at high speeds. A PI controller architecture was employed for consistency with the pitch plane design. The controlled output $\boldsymbol{y}_c$ is the roll attitude ϕ, whereas the reference input $\boldsymbol{r}$ is the roll attitude command ϕ_c. The command error becomes $\boldsymbol{e} = \phi - \phi_c$. Sideslip angle is not considered a controlled output since it is merely regulated by the controller and, thus, appears as part of the state feedback portion of the controller.

For the roll-yaw controller design, the LQR performance index was selected to be

$$J = \int_0^\infty q_3\left[(\varepsilon\phi)^2 + K(\varepsilon\dot{\phi})^2 + q_4(\dot{\beta})^2\right] + (\dot{M}_x)^2 + (\dot{M}_2)^2 \mathrm{d}t \tag{15}$$

The $\varepsilon\phi$ term of Eq. (15) penalizes the roll attitude error to provide command following, the $\varepsilon\dot{\phi}$ term penalizes the rate of change of the command error to control command overshoot, the $\dot{\beta}$ term penalizes sideslip excursions, and the $\dot{M}_x$ and $\dot{M}_z$ terms penalize the control effort employed. The design approach for this controller paralleled that employed for the pitch plane designs. LQR design charts were employed at various points in the flight envelope to select values of K and q_4 in Eq. (15) that allowed the desired stability and transient response characteristics to be achieved with some value of q_3. The value of q_3 was then iterated at each design point to select controller gains that satisfied the design goals.

Thrust Distribution and Limiting

The purpose of the thrust distribution and limiting algorithm is to utilize moment and system thrust commands to compute individual thruster commands satisfying propulsion system constraints. Thrust distribution by itself can be accomplished by a simple matrix multiply. The challenging aspect of this function is to allocate the thrust resources optimally when the moment commands exceed the propulsion system capability. This allocation allows the flight control system (FCS) to prioritize which moments are achieved

(i.e., pitch, yaw, roll) to ensure that the guidance objectives (altitude and MDRC) are satisfied.

If the total system thrust commanded by the flight control system

$$\left(\sum_{i=1}^{4} T_i(t) = T_{\text{sys}}(t)\right)$$

exceeds the total system thrust capability of the PEPS system [$T_{\text{sys}}(t)$ as shown in Fig. 3] the individual thruster commands are reduced until the total thrust commanded equals the PEPS capability. This reduction is made based on an axis prioritization so that guidance and MDRC constraints are satisfied.

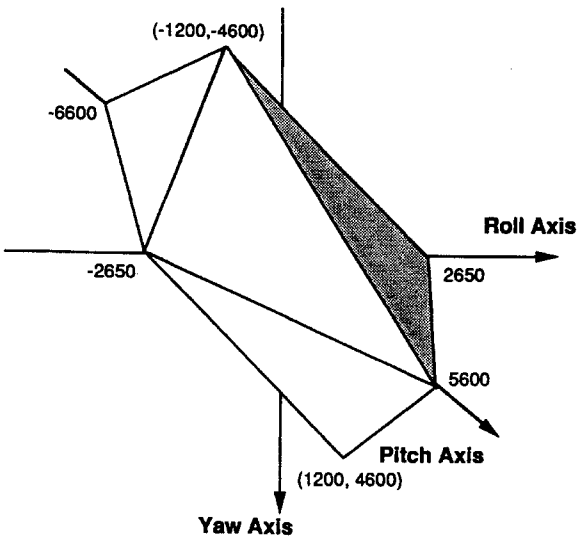

Fig. 7 Maximum achievable moments (foot-pound) from PEPS.

Figure 7 illustrates the moment capability provided by the four-thruster configuration. The propulsion system can satisfy any moment command within the octahedron. If the command lies outside this surface, the goal of the limiting logic is to project it back onto the surface according to a desired moment priority.

This approach employs a two-stage iterative process in which the first stage computes individual thruster commands by solving a set of linear equations and the second stage accomplishes the limiting. The second stage employs logic to test the thruster commands and modify the moment commands, if necessary, for a subsequent iteration. The iterations stop when the thruster commands fall within the thruster limits. A final adjustment is made to take full advantage of the propulsion capability.

The first stage is implemented using a transformation matrix derived from the location and orientation of the thrusters relative to the seat center of gravity. The relationship in matrix form between the thrust and moment command vectors is $\boldsymbol{M} = A\boldsymbol{T}$, where $\boldsymbol{M} = [M_x \;\; M_y \;\; M_z \;\; T_{\text{sys}}]^T$ and $\boldsymbol{T} = [T_1 \;\; T_2 \;\; T_3 \;\; T_4]^T$. Note that the moment command vector is augmented with total system thrust so that the A matrix is square. The fourth row of A contains all ones so that $T_{\text{sys}} = T_1 + T_2 + T_3 + T_4$. Using this formulation, the A matrix can be inverted and used to solve for the thruster command vector as follows: $\boldsymbol{T} = A^{-1}\boldsymbol{M}$.

The second stage tests the four thruster commands to determine if any fall outside the propulsion system limits (150–2500 lb for the PEPS system). If necessary, the moment command vector is modified according to the command priority and a new thruster command vector is computed. When the thruster command is within the limits, a final adjustment is made to place the moment command vector on the surface of the moment capability surface (octahedron).

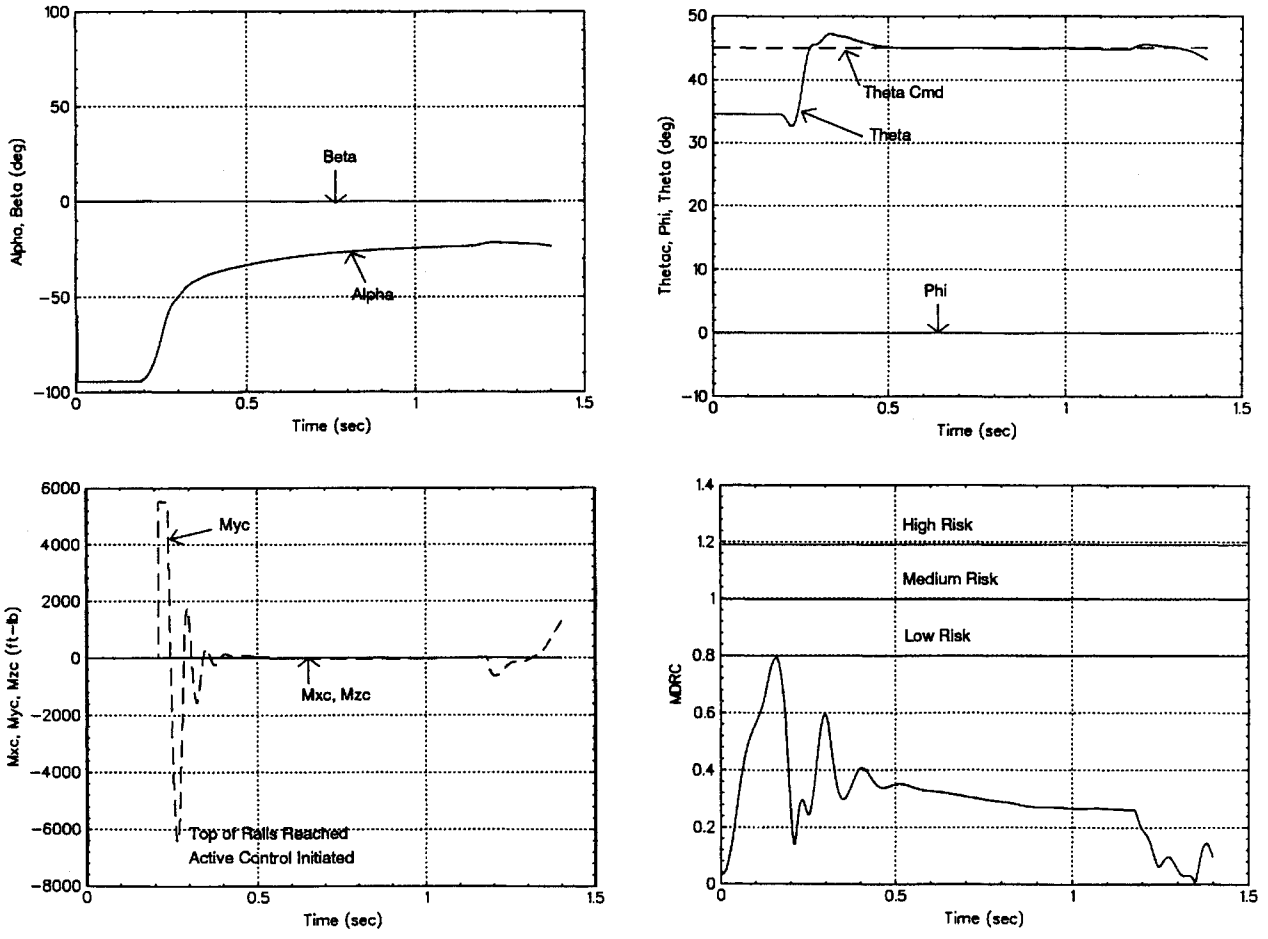

Fig. 8 Static velocity ejection case with pitch attitude control.

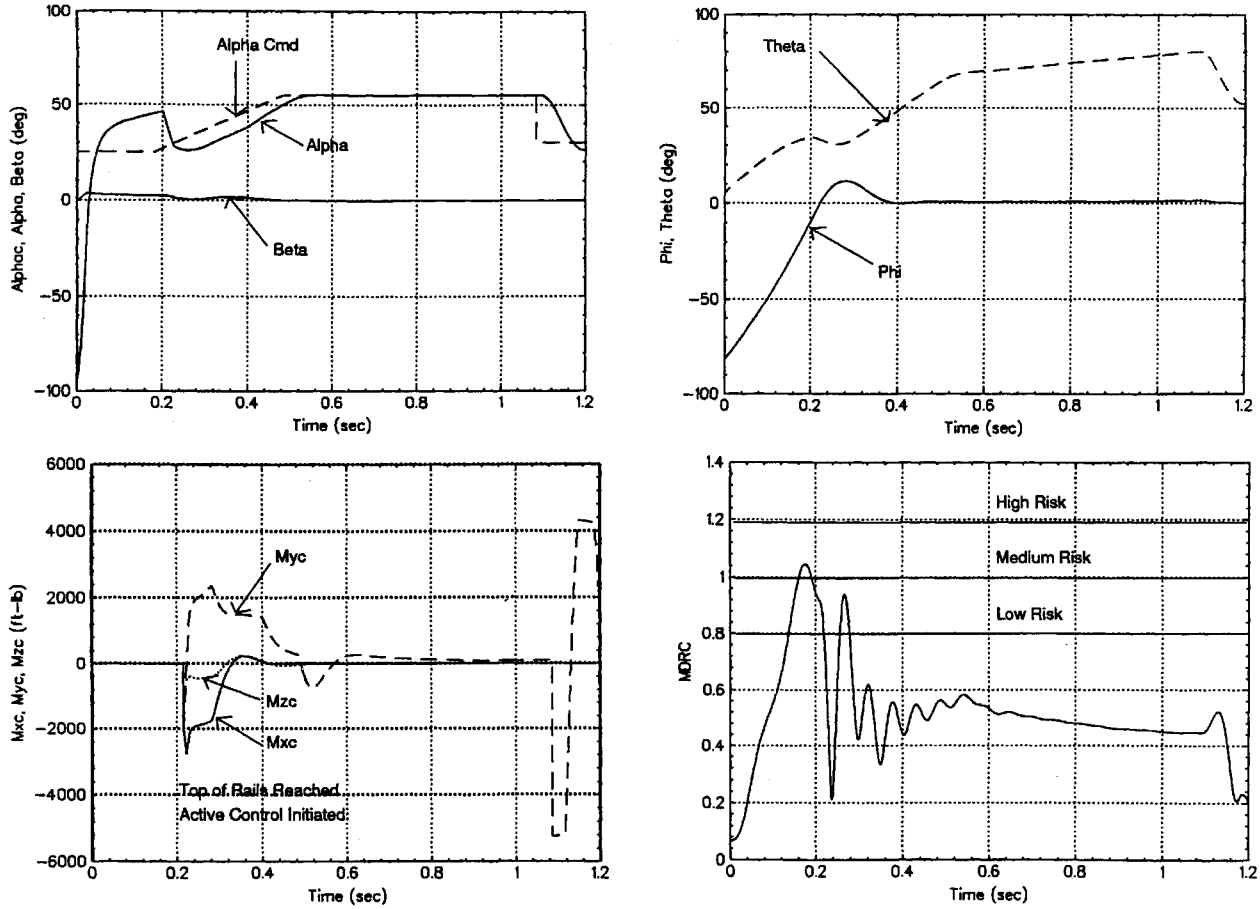

Fig. 9 With AOA control, 450 KEAS and 360-deg/s initial roll rate.

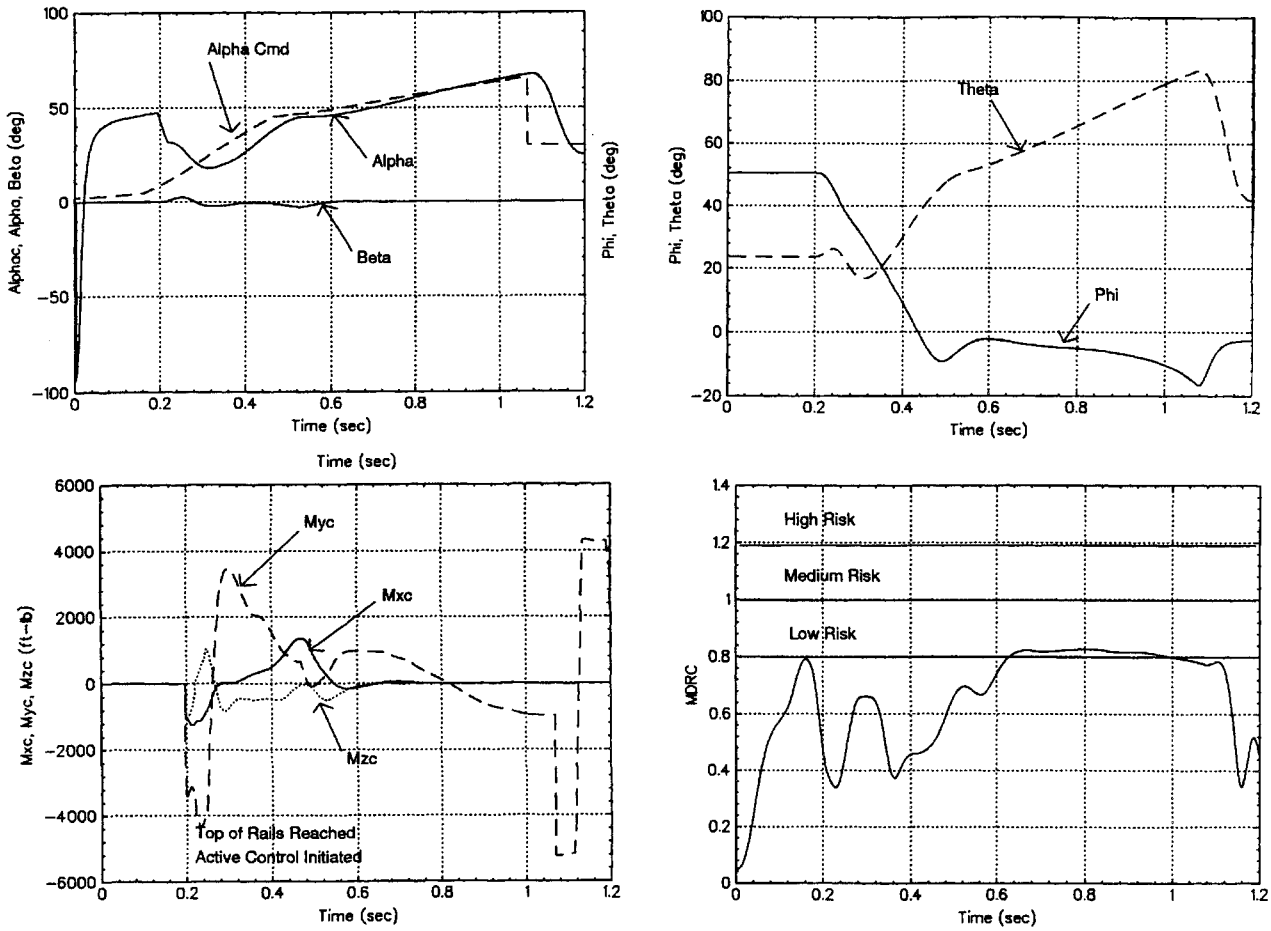

Fig. 10 With AOA control, 700 KEAS and 45-deg initial roll angle.

Control Law Design Results

The performance and stability robustness of the robust servo LQR design was evaluated over a velocity range of 0–700 KEAS, an AOA range from −90 to +90 deg, and a dynamic pressure range of 0–2000 psf. Linear analyses were used to compute stability margins (multivariable gain and phase margins) and to evaluate the time-domain performance for both pitch and roll-yaw control laws (rise time, command overshoot, thrust usage). The conference version of this paper[19] contains a detailed presentation of the linear analysis results. In addition, the LQR PI controller was evaluated in a nonlinear 6-DOF simulation to validate the gain schedules and full envelope system performance. These 6-DOF simulation results are presented here.

The flight control design presented in this paper will undergo flight testing at Holloman Air Force Base in 1996. The three ejection scenarios presented represent planned flight tests. The first scenario is a static ejection, which is the lowest dynamic pressure flight condition. The second scenario is a 450-KEAS initial velocity, 360-deg/s initial roll rate, with the ejection starting at a negative 90-deg roll angle. This represents the most dynamic set of initial conditions. The third scenario is a 700-KEAS ejection with a 45-deg initial roll angle. This represents the highest dynamic pressure flight condition. At this high dynamic pressure it is critical to minimize the aerodynamic sideforce (sideslip angle) on the pilot. These scenarios are presented to illustrate the flight control system performance over its range of dynamic pressure and initial conditions.

Figure 8 displays 6-DOF simulation trajectories for the static ejection (zero velocity). The figure shows time histories for AOA and sideslip, the moments commanded by the control system, body attitudes, and a normalized multiaxial dynamic response criteria (1 = medium risk). At low velocities, body attitudes are controlled to steer the escape system to a safe parachute deployment altitude. The time histories show that the pitch moment command saturates as the seat comes off the rails, thus requiring anti-integrator windup logic. Within 200 ms the seat attitude is accurately tracking the command. The MDRC time history shows that the accelerations experienced during the maneuver represents a low injury risk to the pilot.

Figure 9 displays 6-DOF simulation trajectories for a 450-KEAS initial velocity, 360-deg/s initial roll rate, with the ejection starting at a negative 90-deg roll angle. For this flight condition AOA is controlled to prevent the aerodynamic loads from injuring the pilot, and roll attitude is regulated to steer the escape system (so it climbs vertically). As shown in Fig. 9, the AOA tracks the commanded value and roll attitude is regulated. The steady-state error in tracking the AOA command is a result of the type I controller used in the robust servo LQR. (From classical control, type I controllers track constant commands with zero error. A type II controller would be needed to track a ramp with zero error.) The AOA command is rate limited to help prevent actuator saturation.

Figure 10 displays time histories for the 700-KEAS velocity with 45-deg initial roll angle. The robust servo LQR provides excellent sideslip regulation as the escape system rolls to a vertical attitude. As a result, the MDRC represents a low risk of injury to the pilot.

Conclusions

This paper demonstrates a linear quadratic-based flight control design for an ejection seat equipped with a highly nonlinear solid-fuel pintle propulsion system. Proper selection of the LQR performance index produces a design that balances stability and performance requirements while minimizing required control effort.

Linear analyses of the design showed that the LQ PI controller provides uniform performance across the flight envelope, with only slight degradation at the high-speed, high-AOA flight conditions. Similarly, the control activity was found to be uniform across the flight envelope. Classical control law design techniques provide no direct method for minimizing control usage while meeting performance goals. This is one of the direct benefits of using an optimal control for this application.

Nonlinear simulation was used to verify that the control laws accurately control the escape system. The simulation time histories demonstrate that by accurately controlling the AOA and sideslip angle yields a low risk of serious injury to the pilot can be maintained during the ejection.

References

[1]Schoen, J., "Fourth Generation Escape System Technologies Demonstration Preliminary Design," *Proceedings of the 31st Annual SAFE Symposium* (Reno, NV), SAFE Association, Cottage Grove, OR, 1993.

[2]Zencbi, T., Ayoub, P., Tung, C., and Quartucio, J., "Advanced Technology Crew Station Escape Capsule and Ejection Seat Assessment and Technology Projection," Naval Air Development Center, Rept. NADC-89015-60, Warminster, PA, 1988.

[3]Jines, L. A., and Roberts, E. O., "Enhanced Ejection Seat Performance with Vectored Thrust Capability," Flight Dynamics Lab., Rept. AFAWL-TR-84-3026, Wright–Patterson AFB, OH, 1985.

[4]Jines, L. A., "The Air Force Ejection Seat as a Vehicle for Digital Flight Control," AIAA Paper 83-2205, Aug. 1983.

[5]Reichenau, D., "Aerodynamic Characteristics of a Full-Scale ACES-II Ejection Seat with a Small Female or Large Male Mannequin at Mach Numbers from 0.2 to 1.4," Arnold Engineering Development Center, Rept. AEDC-TR-87-16, Arnold AFB, TN, 1987.

[6]Kolesar, C. E., "Crew Escape Technologies (CREST) Test Results: Half Scale Ejection Seat Tests in the AEDC PWT 16T Transonic Tunnel and AEDC 16S Supersonic Tunnel," Human Systems Div., Air Force Command, Rept. HSD-TP-88-020, Brooks AFB, TX, 1989.

[7]Wise, K. A., "Optimizing Singular Value Robustness Measures in a Conventional Bank-to-Turn Missile Autopilot," *Proceedings of the AIAA Guidance, Navigation, and Control Conference* (Minneapolis, MN), AIAA, Washington, DC, 1988, pp. 296–306.

[8]Wise, K. A., Dierks, M., Kerkemeyer, B., and Tang, J., "Linear and Nonlinear Flight Control for the AIAA Controls Design Challenge," AIAA Paper 92-4628, Aug. 1992.

[9]Doyle, J. C., Francis, B. A., and Tannenbaum, A. R., *Feedback Control Theory*, Macmillan, New York, 1992.

[10]Kwakernak, H., and Sivan, R., *Linear Optimal Control Systems*, Wiley, New York, 1972.

[11]Schoen, J., "CREST Initial Design Report," McDonnell Douglas Corp., DAC Rept. J3846, Oct. 1985.

[12]Keller, R. M., "CREST Trade Study Report, Discussion and Index," McDonnell Douglas Corp., DAC Rept. MDC J3728, June 1985.

[13]Anderson, T., "F/A-18 Hornet Ground Proximity Warning System Design Report," version 3.0 rev. A, Strike Aircraft Test Directorate, NAWC/AD, Sept. 1993.

[14]McRuer, D., Ashkenas, I., and Graham, D., *Aircraft Dynamics and Automatic Control*, Princeton Univ. Press, Princeton, NJ, 1973.

[15]Pickl, W., Carlson, R., Tam, W., and Wallace, B., "Improving Escape Capsule Performance Using Active Pitch Control," *Proceedings of the 32nd Annual SAFE Symposium* (Reno, NV), SAFE Association, Cottage Grove, OR, 1994, pp. 264–274.

[16]Davidson, E. J., and Copeland, B., "Gain Margin and Time Lag Constraints Applied to the Stabilization Problem and Robust Servomechanism Problem," *IEEE Transactions on Automatic Control*, Vol. AC-30, No. 3, 1985, pp. 229–239.

[17]Williams, D. E., Friedland, B., and Madiwale, A. N., "Modern Control Theory for Design of Autopilots for Bank-to-Turn Missiles," *Journal of Guidance, Control, and Dynamics*, Vol. 10, No. 4, 1987, pp. 378–386.

[18]Wise, K. A., "Bank-to-Turn Missile Autopilot Design Using Loop Transfer Recovery," *Journal of Guidance, Control, and Dynamics*, Vol. 13, No. 1, 1990, pp. 145–152.

[19]Wise, K. A., and Brinker, J. S., "Linear Quadratic Flight Control for Ejection Seats," AIAA Paper 95-3320, Aug. 1995.